

1
2
3
4
5
6
7
8
9
10
11
12
13
14
15
16
17
18
19
20
21

REVISION 1

Total word count = 3,482

On the Formation of Arrays of micro-Tunnels in Pyrope and Almandine Garnets

Jacques Rabier¹, Arthur H. Heuer² and Kevin J. Hemker^{3*}

¹ Département Physique et Mécanique des Matériaux, Institut Pprime, , CNRS-Université de Poitiers, ISAE ENSMA, BP 30179, 86962 Futuroscope-Chasseneuil Cedex 05, France

² Department of Materials Science and Engineering, Case Western Reserve University, Cleveland, Ohio, United States of America

³ Departments of Mechanical Engineering, Materials Science and Engineering, Earth and Planetary Sciences, Johns Hopkins University, Baltimore, MD, 21210 United States of America

* Corresponding author
Email: hemker@jhu.edu

22 **Abstract**

23 A recent paper devoted to unusual fine-scale tubular tunnels found in pyrope and
24 almandine garnets suggested that the 5 to 100 micron diameter tunnels were produced by an
25 endolithic organism that is able to chemically dissolve and penetrate the mineral, perhaps in
26 search of nutrients. The hypothesized microbial boring of the garnets was based on the
27 finding of endolithic remains in the tunnels, but boring alone does not adequately explain the
28 linear, highly aligned or occasionally branched tunnels that have been imaged. We have
29 prepared this short Letter, in the spirit of *Occam's Razor*, to highlight the very probable role
30 that dislocations play in the creation of such tunnels by preferential etching of a dislocation-
31 rich deformation microstructure. The geometrical features of the tunnels possess all the
32 characteristics of classical dislocation substructures that have been observed in natural and
33 synthetic garnets.

34

35 **Introduction**

36 The intricate and beautiful X-ray computed tomographic images recently published by
37 Ivarsson *et al.* (2018) contain clear evidence of highly aligned parallel tunnels that originate at
38 the mineral surface and extend into the interior, see for example Figure 1. These tunnels form
39 highly regular miniature palisades in some regions; in others, they exist as more chaotic
40 branched networks with kinks and junctions with uniquely prescribed angles. The networks of
41 curvilinear, branching and anastomosing (interconnected) tunnels were interpreted as
42 evidence that these tunnels are independent of crystallography, thus providing an indirect
43 foundation for the authors' hypothesis of biological tunneling (Ivarsson *et al.* 2018).
44 Unfortunately, this interpretation completely misses the striking geometric similarities
45 between the tunnels in these tomographic images and published observations and

46 understanding of dislocation microstructures in both natural and synthetic garnets -- see for
47 example, Rabier (1995); Rabier *et al.* (1976); Rabier (1979); Rabier *et al.* (1981); Garem *et*
48 *al.* (1982); Rabier and Garem (1984); Allen *et al.* (1987); Karato *et al.* (1995); Blumenthal
49 and Phillips (1996); Voegelé *et al.* (1998 a,b).

50 **[Insert Figure 1]**

51 As is well known, dislocations are prominent in virtually all crystalline materials.
52 Dislocation generation, multiplication, and motion is widely recognized as a common
53 deformation response of crystalline materials to externally applied shear stresses, and have
54 been extensively observed and characterized in metals and alloys, minerals, ceramics, and
55 semiconductors. The absence of dislocations in the pyrope and almandine garnets under
56 discussion, if true, would be remarkable.

57 Here, we briefly review and discuss dislocations in garnets, tunnel formation due to
58 abiogenic etching of dislocations in minerals, and the similarities between the geometry of
59 dislocation substructures and the intricate tunnels and networks observed in these pyrope and
60 almandine garnets (Ivarsson *et al.* 2018).

61

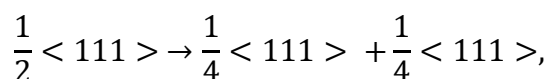
62 **Dislocations in garnets**

63 The relationship between dislocations and plasticity in garnets is well established.
64 Synthetic garnets of technological interest such as $Y_3Al_5O_{12}$ (YAG, yttrium aluminum
65 garnet), $Y_3Fe_5O_{12}$ (YIG, yttrium iron garnet) and $Gd_3Ga_5O_{12}$ (GGG, gadolinium gallium
66 garnet) were first studied by Rabier and colleagues (Rabier J, Garem H, and Veysiere P.
67 1976, Rabier J. 1979) and have exceptional plastic properties compared to other oxide crystals
68 (Garem *et al.* 1982; Rabier and Garem, 1984; Blumenthal and Phillips 1996). Likewise, the
69 resistance to plastic deformation in natural garnets is significantly greater than that of most

70 other minerals of the Earth's mantle (Karato *et al.* 1995; Voegelé *et al.* 1998a). This is related
71 to the very large Burgers vectors of dislocations in garnets, and to a “corrugated” oxygen
72 sublattice, which promotes very high atomic-level friction stresses on moving dislocations.

73 The description of the garnet structure in terms of coordination polyhedra, so common
74 in the mineralogical literature, has proven to be very useful in understanding dislocation
75 properties in synthetic garnets (Rabier J, Veysiere P, and Grilhé J. 1976b). The garnet
76 structure can be regarded as a body centered cubic (bcc) lattice with a very large unit cell. The
77 edge of the bcc unit cell is of order 1.2 nm, whereas most common minerals have
78 considerably smaller unit cells. Thus, the magnitude of the smallest perfect unit Burgers
79 vector, $\mathbf{b} = \frac{1}{2}\langle 111 \rangle$, is about 1.0 nm. This results in a very large strain energy, proportional to
80 Gb^2 per unit length of dislocation (G is the elastic shear modulus). The strain energy of a
81 dislocation can be lowered by spreading of its core and by dissociation of the parent
82 dislocation into partial dislocations that bound a planar stacking fault. The dissociated
83 configuration is glissile as long as it remains on the glide plane, but it becomes sessile when
84 reconfigured off of the glide plane (Garem *et al.* 1982; Blumenthal and Phillips 1996).

85 In synthetic garnets, perfect dislocations have been shown to dissociate into co-linear
86 partial dislocations according to the reaction



87 (Rabier *et al.* 1976b; Rabier *et al.* 1981), in grossularite ($\text{Ca}_{2.9}\text{Fe}_{0.2}\text{Al}_{1.9}\text{Si}_3\text{O}_{12}$) (Allen *et al.*
88 (1987) and in gem quality single crystal garnet (Voegelé *et al.* (1998a) and in a variety of
89 natural samples (Voegelé *et al.* 1998b). Even with this dissociation, the partial dislocations
90 have very large strain energies that have important consequences for the observed dislocation
91 microstructures. The work of Rabier *et al.* already cited has shown that dislocations are
92 clearly aligned along the screw direction in synthetic garnet single crystals that have

93 undergone high temperature deformation up to moderate strain; this appears not to be the case
94 for the natural garnet deformed under hydrostatic confining pressures at elevated temperatures
95 (Voegelé *et al*, 1998a). Finally, the large unit cells in garnets make possible the formation of
96 hollow dislocation cores, as suggested by Nabarro (1984).

97 A representative micrograph is shown in Figure 2a; it was taken from a $Gd_3Ga_5O_{12}$ (GGG)
98 single crystal that had been deformed in compression along [100] at 1350°C (0.81 of the
99 absolute melting temperature, T_M) to a strain of 0.4% at a strain rate of 3.3×10^{-6} /s (Rabier
100 1979). The two most prominent dislocations in this figure are clearly aligned along $\langle 111 \rangle$
101 and thus are in a screw orientation. Moreover, the rapid transition to screw character from the
102 source pinning point (upper white arrow) further attests to the anisotropy of dislocation glide
103 in this material. The micrograph in Figure 2b shows dislocations in GGG that had been
104 compressed along [110] to a plastic strain of 0.1% at 1450°C (0.86 T_M) at a strain rate of
105 3.3×10^{-6} /s. Here, dislocation glide loops are segmented along orientations corresponding to
106 both screw and mixed character. In Fig. 2b, the vector **b** is the projection of the Burgers
107 vector $\frac{1}{2} [1-11]$ and the straight dislocation parallel to it is a screw dislocation.

108 **[Insert Figure 2]**

109 Studies have also shown that dislocation glide in garnets occurs on {110}, {112}, or
110 {123} slip planes and that the plane with the highest resolved shear stress is not always
111 activated. This violation of the Schmid law (Rabier and Garem 1984), which describes the
112 geometric relationship between the applied stress and the shear stress resolved onto specific
113 slip planes, is analogous to what is found in bcc metals at low temperatures and may be taken
114 as another indication of the effect of dislocation character on dislocation mobility.

115 In bcc metals, screw dislocations have non-planar cores and are difficult to move,
116 while edge and mixed character dislocations remain planar and are relatively easy to move.

117 The consequence is that the more mobile dislocations run out and are underrepresented in the
118 dislocation substructure, resulting in a preponderance of crystallographically oriented, long,
119 straight screw segments. In bcc metals, thermal activation of the screw dislocations facilitates
120 a transformation from “low” to “high” temperature deformation microstructures involving the
121 disappearance of long screw dislocation segments. By contrast, the screw dislocations in
122 synthetic garnets remain immobile even at high temperatures owing to the magnitude of their
123 Burgers vector. At high temperatures, in addition to straight screw segments, rectilinear
124 mixed and edge character dislocation segments, resulting from diffusive climb dissociation
125 out of the glide plane, can also be found. Diffusive climb of edge and mixed dislocations out
126 of their glide planes also leads to the presence of curved dislocations (Rabier 1995), and the
127 final result is that both straight and curved dislocation segments can co-exist in garnets that
128 have undergone high temperature plastic deformation. Lastly, we note that deformation by
129 pure dislocation climb in garnets may also be important in mantle dynamics (Ritterbex *et al.*
130 (2020).

131 The dislocation microstructures that form in natural garnets are the result of geological
132 heating and stresses and the thermo-mechanical deformation that ensues at elevated
133 temperatures. Once cooled, the dislocation structures are frozen into the crystals, and
134 subsequent “decoration” of the dislocations by impurities or the formation of etch tunnels
135 along the dislocation lines can occur, with the natural consequence that the tunnels and
136 impurities will maintain the network topology of the underlying dislocation substructure.

137

138 **Etched tunnels arising from dislocations in minerals**

139 It is well known that the localized strain fields associated with dislocations affect the
140 reactivity of the material by providing favorable areas for chemical reactions such as

141 precipitation and dissolution. They also provide rapid diffusion paths for ingress of fresh
142 reactants. The formation of etch tunnels along dislocations after specific treatments has been
143 documented in a number of minerals, *e.g.* quartz (SiO₂), forsterite (Mg₂SiO₄), and olivine
144 (Mg,Fe)₂SiO₄ - see for example Tingle and Green (1992). The decoration of dislocations in
145 forsterite (Jaoul *et al.* 1979) and olivine (Karato 1987) has been used to study the dislocation
146 microstructures of these materials, and a comprehensive description of these dislocation
147 microstructures has improved our understanding of the thermo-mechanical properties of
148 these minerals.

149 As far as garnets are concerned, similar observations of etched dislocations have also
150 been reported. Dislocation microstructures in pyropes were revealed by HF etching by
151 Carstens (Carstens 1969). Studying the elongated shapes of garnets in high-grade
152 metamorphic rocks, Azor *et al.* (1997) concluded that “dislocation-enhanced dissolution,
153 which occurs at low temperatures and low dislocation mobility, is arguably the mechanism
154 responsible for partially dissolving the garnet grains”. Recently Liu *et al.* (2018) presented a
155 new method for decorating dislocations in garnets based on a pre-melting decoration process.
156 This work indicated that the decorated lines were generated by a pre-melting reaction that
157 occurred along the dislocation cores of individual dislocations and low-angle sub-grain
158 boundaries, which are essentially an ordered array of dislocations. These experiments clearly
159 show that a number of abiogenic processes can naturally lead to etched tunnels along
160 dislocations in garnets.

161 Ivarsson *et al.* (2018) performed time-of-flight SIMS analyses of freshly fractured
162 surfaces of their garnets and reported high organic content (fatty acids) localized to newly
163 exposed tunnels. They interpreted this as the physical and chemical remains of endolithic
164 microorganisms within the tunnels, and they further hypothesized that the tunnels were the
165 result of microbially mediated boring of the garnets for nutritional reasons. The geometrical

166 precision inherent to the palisades and interconnecting networks that were elucidated by
167 Ivarsson *et al.* would be hard to maintain while tunneling through an opaque solid. Moreover,
168 it is important to note that the finding of organic content in the tunnels is also fully consistent
169 with the abiogenic etching of dislocation substructures and subsequent habitation of the
170 tunnels by endoliths.

171

172 **Intricate tunnels in Thai garnets from soils and river sediments**

173 Most if not all of the tunnel-like geometrical features exhibited in the work of Ivarsson
174 *et al.* (2018) can be explained by dislocation theory. Correlation with location-specific
175 crystallographic orientation maps, which is now possible with state-of-the-art electron
176 microscopes, would allow for direct confirmation or refutation of the role of dislocations, but
177 the following observations and comparisons are very convincing on their own.

178 The findings of Ivarsson *et al.* that the tunnels all originate from the mineral surfaces
179 and extend into the mineral interiors points to the role of an external etchant or agent, as
180 suggested by the authors. However, it is also important to recognize that dislocations cannot
181 end within a grain and must terminate at exterior surfaces, interior grain or phase boundaries,
182 or by making junctions with other dislocations. For example, the short lines in Figure 2 are
183 inclined dislocations that intersect the top and bottom surfaces of the thin electron-transparent
184 TEM foils that were prepared from plastically deformed garnet samples. Moreover, the
185 emergent point where a dislocation intersects a free surface is known to be more reactive, and
186 when etched, has geometrical features that reflect the underlying crystal symmetry. The
187 observation that most tunnels in the images of the garnets published in Ivarsson *et al.* (2018)
188 have hexagonal cross-sectional symmetry is fully consistent with the presence of screw

189 dislocations aligned along $\langle 111 \rangle$ crystallographic orientations. Similarly, the minority of
190 tunnels that have rectangular cross-sections are easily explained by the presence of a smaller
191 number of edge and mixed dislocations.

192 The straight and highly parallel and aligned nature of the miniature palisades and
193 tunnels in Figs. 1B and 3A-E of Ivarsson *et al.* (2018) are very striking and also very
194 suggestive of screw dislocation microstructures. Measuring the orientation of individual
195 grains should be undertaken to confirm or disprove the relation of the tunnels to screw
196 dislocations, and this would further support the evidence provided by the hexagonal cross-
197 sections. Knowing the grain orientation would also allow development of a quantitative
198 model of the very regular kink angles that have been observed, suggestive of either
199 dislocations lying along two intersecting $\langle 111 \rangle$ directions or a single dislocation with
200 adjacently locked screw, mixed or edge character segments, similar to what is shown in Fig
201 2B. We further note that qualitative measures such as observable tunnel densities (in the
202 range of 10^7 - 10^{10} tunnels per square meter) are comparable to dislocation densities that are
203 associated with modest amounts of plastic deformation.

204 The more complex curved and branching microstructures shown in Figs. 1C, 2A and
205 4A in Ivarsson *et al.* (2018) that form deeper in the grains led Ivarsson *et al.* to disregard any
206 crystallographic influence on the formation of the tunnels, but these too are easily explained
207 by the presence of dislocations. Curved tunnels most likely form from mixed dislocations, or
208 dislocations that have undergone diffusive climb out of their glide plane. Branching of the
209 tunnels is analogous to dislocation microstructures that arise from elastic interactions that
210 create dislocation junctions and networks, and that involve several families of interacting
211 dislocations. Ivarsson *et al.* have pointed out the similarity of the connecting branches they
212 observed (*e.g.* their Fig. 4A) to anastomoses (interconnections) that are observed in biological
213 systems such as blood vessels and leaf veins, but such segments and junctions are also

214 commonly formed and observed in dislocation networks. For example, Rabier *et al.* (1976b)
215 have shown that dislocation junctions with connecting segments of $\langle 100 \rangle$ and $\langle 110 \rangle$ Burgers
216 vectors result from the interaction of two families of dislocations with $\frac{1}{2} \langle 111 \rangle$ and
217 $\frac{1}{2} \langle 11\bar{1} \rangle$ Burgers vectors in $Y_3Fe_5O_{12}$ (YIG) deformed at 1350 °C, see for example Fig. 3.
218 The narrowing and eventual termination of the tunnels in the grain interior of the Thai garnets
219 is an indication that the etching or attack that starts on the surface had not run to completion.

220 **[Insert Figure 3]**

221 **Implications**

222 The intricate tunnels imaged in pyrope and almandine garnets found in soils and river
223 sediments (Ivarsson *et al.* 2018) can be fully explained, without straining credulity, by
224 abiogenic etching of dislocation microstructures contained within the minerals. There are
225 striking geometric similarities between these tunnels and dislocation networks that have been
226 observed and published in numerous natural and synthetic garnets, and further studies
227 involving local crystallographic orientation mapping via electron backscatter diffraction
228 (EBSD) or similar techniques would be highly informative.

229

230 **Acknowledgments**

231 We thank R. Mittal (Dept. of Mechanical Engineering, Johns Hopkins University) for
232 bringing Ivarsson *et al.* (2018) to the attention of KJH, to D. Beaufort and A. Meunier
233 (IC2MP, Univ. of Poitiers) for discussions with JR concerning biogenic interactions with
234 minerals, and P. Cordier (Univ. of Lille) for helpful comments as a reviewer of an earlier
235 version of this paper.

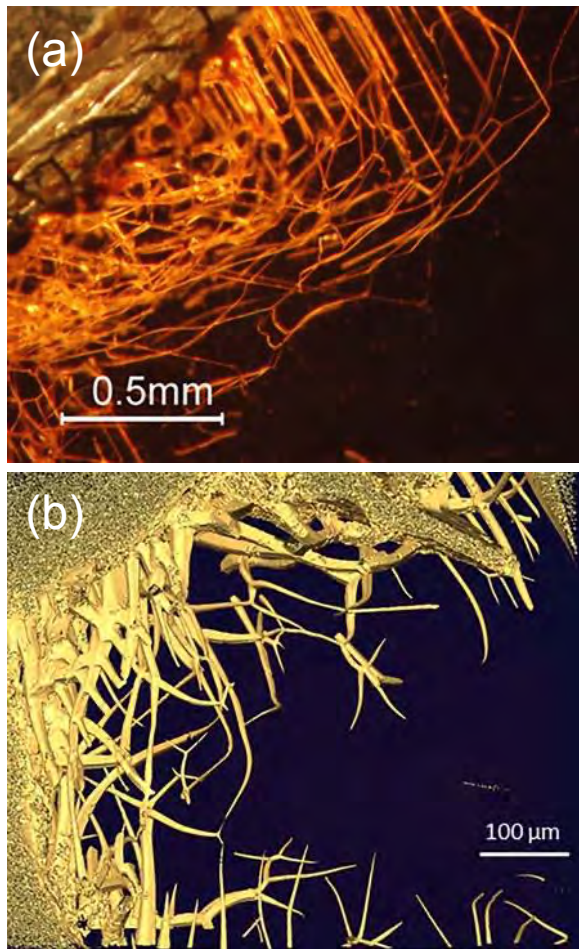
236

237 **References**

- 238 Allen FM, Smith BK, Buseck PR. Direct Observation of Dissociated Dislocations in
239 Garnet. *Science*. 1987;238(4834):1695-7.
- 240 Azor A, Simancas JF, Exposito I, Lodeiro FG, Martinez Poyatos DJ. Deformation of
241 garnets in a low-grade shear zone. *Journal of Structural Geology*. 1997;19(9):1137-48.
- 242 Blumenthal WR, Phillips DS. High-Temperature Deformation of Single-Crystal Yttrium-
243 Aluminum Garnet (YAG). *Journal of the American Ceramic Society*. 1996;79(4):1047-52
- 244 Carstens H. Dislocation structures in pyropes from Norwegian and Czech garnet
245 peridotites. *Contributions to Mineralogy and Petrology*. 1969;24(4):348-53.
- 246 Garem H, Rabier J, Veysière P. Slip systems in gadolinium gallium garnet single
247 crystals. *Journal of Materials Science*. 1982;17(3):878-84.
- 248 Ivarsson M, Skogby H, Phichaikamjornwut B, Bengtson S, Siljeström S, Ounchanum P, *et*
249 *al.* Intricate tunnels in garnets from soils and river sediments in Thailand – Possible
250 endolithic microborings. *PLoS ONE*. 2018;13(8):e0200351.
- 251 Jaoul O, Michaut M, Gueguen Y, Ricoult D. Decorated dislocations in forsterite. *Physics*
252 *and Chemistry of Minerals*. 1979;5(1):15-9.
- 253 Karato S. Scanning electron microscope observation of dislocations in olivine. *Physics*
254 *and Chemistry of Minerals*. 1987;14(3):245-8.
- 255 Karato S-I, Wang Z, Liu B, Fujino K. Plastic deformation of garnets: systematics and
256 implications for the rheology of the mantle transition zone. *Earth and Planetary Science*
257 *Letters*. 1995;130(1):13-30.
- 258 Liu X, Xie Z, Jin Z, Li Z, Ao P, Wu Y. New method for revealing dislocations in garnet:
259 premelting decoration. *Physics and Chemistry of Minerals*. 2018;45(8):925–933
- 260 Nabarro FRN. (1984) Dislocation cores in crystals with large unit cells in *Dislocations*
261 1984. Editions du CNRS, P. Veysière, L. Kubin, J. Castaing Eds.
- 262 Rabier J. Dissociation des dislocation dans les oxydes de structure grenat, Application a
263 l'étude de la déformation plastique de fer d'yttrium (YIG): University of Poitiers; 1979.
- 264 Rabier J. Plastic deformation and dislocations in ceramic materials. *Radiation Effects and*
265 *Defects in Solids*. 1995;137(1-4):205-12.
- 266 Rabier J, Garem H. Plastic Deformation of Oxides with Garnet Structure. In: Tressler RE,
267 Bradt RC, editors. *Deformation of Ceramic Materials II*. Boston, MA: Springer US; 1984.
268 p. 187-98.
- 269 Rabier J, Garem H, Veysière P. Transmission electron microscopy determinations of
270 dislocation Burgers vectors in plastically deformed yttrium iron garnet single crystals.
271 *Journal of Applied Physics*. 1976a;47(11):4755-8.

- 272 Rabier J, Veyssière P, Grilhé J. Possibility of stacking faults and dissociation of
273 dislocations in the garnet structure. *physica status solidi (a)*. 1976b;35(1):259-68.
- 274 Rabier J, Veyssière P, Garem H. Dissociation of dislocation with $a/2 \langle 111 \rangle$ Burgers
275 vectors in YIG single crystals deformed at high temperature. *Philosophical Magazine A*.
276 1981;44(6):1363-73.
- 277 Rabier J, Veyssière P, Garem H, Grilhé J. Sub-grain boundaries and dissociations of
278 dislocations in yttrium iron garnet deformed at high temperatures. *Philosophical Magazine*
279 *A*. 1979;39(6):693-708. K
- 280 Ritterbex, S., Carrez Ph., and Cordier P. Deformation across the mantle transition zone: A
281 theoretical mineral physics view. *Earth and Planetary Science Letters*, 547, 116438
282 (2020). <https://doi.org/10.1016/j.epsl.2020.116438>
- 283 Tingle ER, Green HW II. Formation of fluid inclusions and etch tunnels in olivine at high
284 pressure. *American Mineralogist*. 1992;77(96):296-302.
- 285
- 286 Voegelé V., Ji, Ando JI, Cordier P. and RC. Liebermann Plastic deformation of silicate
287 garnets I. High pressure experiments - *Physics of the Earth and Planetary Interiors*, 108,
288 305-318 (1998a). [https://doi.org/10.1016/S0031-9201\(98\)00110-1](https://doi.org/10.1016/S0031-9201(98)00110-1)
- 289
- 290 Voegelé V Cordier P, Sautter V, Lardeaux JM, Sharp T.G. and Marques FO. Plastic
291 deformation of silicate garnets II. Deformation microstructures in natural samples. *Physics*
292 *of the Earth and Planetary Interiors*, 108, 319-338 (1998b). [https://doi.org/10.1016/S0031-](https://doi.org/10.1016/S0031-9201(98)00111-3)
293 [9201\(98\)00111-3](https://doi.org/10.1016/S0031-9201(98)00111-3)
- 294
- 295

Figure 1

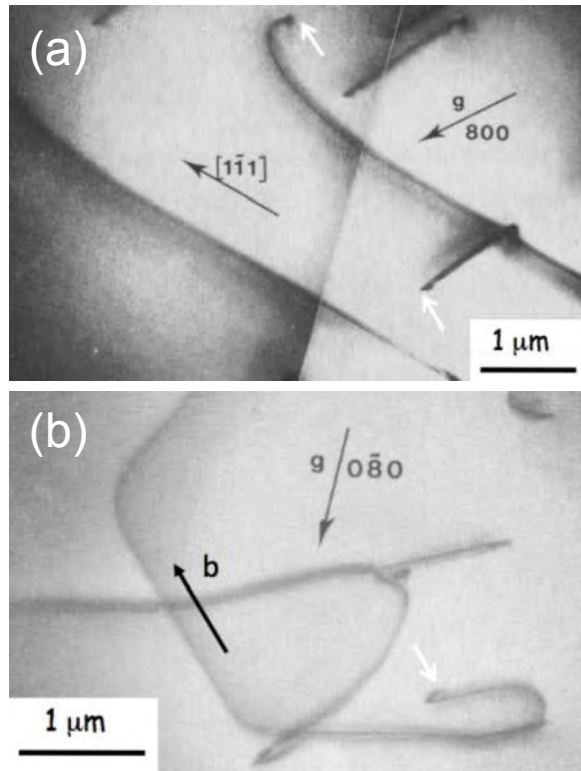


296

297 **Figure 1. Intricate tunnels in pyrope garnets, taken from Ivarsson et al. (2018).** (a) A
298 network of highly parallel and wandering tunnels that originate at the mineral surface and
299 extend into the interior. (b) Tomographic isosurface reconstruction of another garnet with
300 tunnels of defined cross-section. These tunnels originate at the surface, intersect and
301 branch at repeatable angles, and taper to a point as they extend into the interior.

302

Figure 2

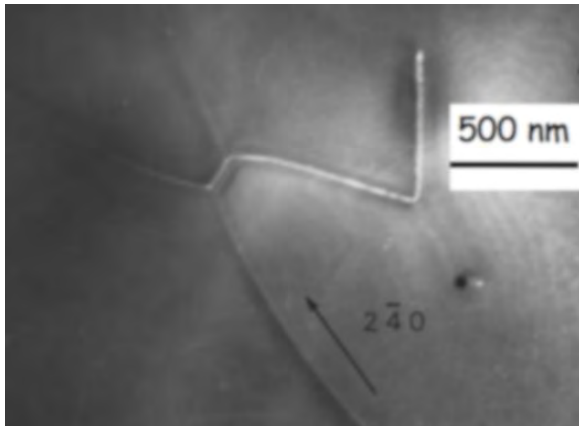


303

304 *Figure 2. TEM micrographs of dislocations in synthetic garnets illustrate a*
305 *preponderance for straight dislocations that are aligned along specific crystallographic*
306 *directions. (a) Long, straight screw dislocations in single-crystalline $Gd_3Ga_5O_{12}$ (GGG)*
307 *that was deformed to 0.4% strain at 1350°C. The short dislocations are also straight; their*
308 *length is simply truncated by intersection with the top and bottom surfaces of the TEM thin*
309 *foil. Examples of surface intersections are noted with white arrows. At lower magnification*
310 *in a bulk crystal, long-straight screw dislocations would align to create an array similar to*
311 *what is shown in Figure 1a. (b) Glide loops are commonly observed to be segmented into*
312 *carefully-aligned screw and mixed dislocation segments imaged in GGG compressed to*
313 *0.1% strain at 1450°C. The mixed dislocations curve and wind in a manner similar to the*
314 *wandering tunnels in Figure 1a.*

315

Figure 3



316

317 ***Figure 3. TEM observations of dislocation junctions, which lead to branching and***
318 ***aligned palisades in synthetic garnets. <100> junctions resulting from the interaction of***
319 ***two <111> dislocation slip systems in Y₃Fe₅O₁₂ (YIG) that had been deformed at 1350°C.***
320 ***These intersections are analogous to the geometrical branching shown in Figure 1b.***

321